Planetary and Space Science 104 (2014) 295–309

Contents lists available at ScienceDirect

Planetary and Space Science

journal homepage: www.elsevier.com/locate/pss

Mineralogy of V-type asteroids as a constraining tool of their past history

S.F.A. Batista [a,b,c,*,1], T.M. Seixas [a,c], M.A. Salgueiro da Silva [a,c], R.M.G. de Albuquerque [a]

[a] Departamento de Física e Astronomia da Faculdade de Ciências da Universidade do Porto, Rua do Campo Alegre, 687, 4169-007 Porto, Portugal
[b] Centro de Astrofísica da Universidade do Porto, Rua das Estrelas, 4150-762 Porto, Portugal
[c] Centro de Investigação da Terra e do Espaço da Universidade de Coimbra, Av. Dr. Dias da Silva, 3000-134 Coimbra, Portugal

ARTICLE INFO

Article history:
Received 17 April 2014
Received in revised form
22 October 2014
Accepted 23 October 2014
Available online 4 November 2014

Keywords:
Vesta
Vestoids
HED meteorites
Mineralogy
Parent bodies

ABSTRACT

In the past few years, the genetic relationship between (4) Vesta, Vestoids and HED meteorites was reinforced (Drake, 2001, Meteorit. Planet. Sci. 36 (4), 501–513). It is believed that Vestoids and HED meteorites were originated from a collision suffered by (4) Vesta, during the early stages of the Solar System. Due to the effects of dynamical resonances, several fragments of this collision were ejected into near-Earth orbits and some of them have originated the so-called HED meteorites. We aim to infer about the hypothetical collision suffered by (4) Vesta and its connection to the genetic relationship between V-type asteroids and HED meteorites. For this purpose, reflectance spectra of a set of 11 V-type asteroids and 55 HED meteorites were obtained, respectively, from the publically available MIT-UH-IRTF Joint Campaign for NEO Reconaissance and RELAB database.

Initially, for each of the selected V-type asteroids, we attempted to identify its meteoritic analogue. Afterwards, we have performed a numerical spectral analysis based on the Hapke radiative transfer model. We report the inferred surface composition and mineralogy of the V-type asteroids, for which we have identified a meteoritic analogue.

Our results strength the relationship between HED meteorites and V-type asteroids, as also suggested by the results from the Dawn mission (de Sanctis et al., 2012, Science, 336 (6082), 697–690; 2013 Meteorit. Planet. Sci. 48 (11) 2166–2184; McSween et al., 2011, Space Sci. Rev. 163 (1–4), 141–174; 2013, Meteorit. Planet. Sci. 48 (11) 2090–2104). The latter is contradicting the results from Schiller et al. (2011, Astrophys. J. 740 L22) and Wasson (2013, Earth Planet. Sci. Lett. 381 138–146), which questioned this linkage. We also report the best meteoritic kind for the studied V-type asteroids, by comparing their spectra and mineralogies. We also report the pyroxenes mineralogical distributions of the HED meteorites, inferred through the Hapke radiative transfer model, which can be suitable for comparison with future mineralogical studies of these objects.

1. Introduction

Establishing possible linkages between asteroids and meteorites is of crucial importance as they allow us to understand the compositional and thermal gradients in the solar nebula. A topic of interest is the history of very early nebular solids, which provide important constraints on nebular conditions and processes fundamental to astrophysical models of nebular evolution. A discussion about possible parent bodies across the diversity of meteorites is provided by Burbine et al. (2002).

(4) Vesta is quoted to be a surviving differentiated protoplanet (Russell et al. 2012). According to spectral data, orbital dynamics studies and remote sensing data from the DAWN mission, the genetic relationship between HED meteorites and (4) Vesta has been reinforced during the last few years (McCord et al., 1970; Binzel and Xu, 1993; Binzel et al., 1997; Drake, 2001; de Sanctis et al. 2012, 2013; McSween et al. 2011, 2013). But, this linkage was early questioned (Wasson and Wetherill, 1979). Indeed, recently there are some authors still questioning this linkage (see, e.g., Schiller et al., 2011; Wasson, 2013). In one hand, Schiller et al. (2011) discuss that the ^{26}Mg* variations in eucrites and diogenites imply that near complete solidification of the HED parent body occurred in a short timescale of 2–3 Myr. According to thermal

* Corresponding author.
E-mail addresses: s.f.assuncaobatista-1@tudelft.nl (S.F.A. Batista), tmseixas@fc.up.pt (T.M. Seixas).
[1] Current address: Faculty of Aerospace Engineering, Technical University Delft, Kluyverweg 1, 2629 HS Delft, The Netherlands.

http://dx.doi.org/10.1016/j.pss.2014.10.012
0032-0633/

models, the latter rapid cooling and magma ocean crystallization could only take place in small asteroids with a dimension inferior to 100 km. On the other hand, Wasson (2013) argue that spectral similarities between (4) Vesta and HED meteorites are not enough to establish a genetic linkage between both. Wasson (2013) also argues that more than half of the V-type asteroids do not belong to the so-called Vesta dynamical family. Wasson (2013) concludes that HED are not from Vesta, but may come from the same parent body as pallasites and IIIAB irons.

The surface of (4) Vesta exhibits strong absorption features near 0.9 and 1.9 μm, evidencing the presence of Fe-bearing pyroxenes. Data obtained with the Dawn VIR instrument revealed, however, large variations in pyroxenes mineralogies (de Sanctis et al., 2012, 2013). The VIR spectra is consistent with a surface mineralogy similar to howardites (de Sanctis et al., 2012, 2013), confirming the evidence pointed out by Hiroi et al. (1995). Nevertheless, the regolith of (4) Vesta also contains varying proportions of eucritic and diogenitic materials, at different locations (de Sanctis et al., 2013). Olivine was also detected in the Nothern hemisphere of (4) Vesta (Ammannito et al., 2013). The giant impact suffered by (4) Vesta, which formed the Rheasilvia basin, excavated a large amount of eucritic and diogenitic material (Takeda 1997) and redistributed it over the surface. The mineralogical composition of the deepest layers of the basin are dominated by orthopyroxene-rich materials (de Sanctis et al. 2013).

(4) Vesta is close to the 3:1 jovian and υ_6 resonances, which may be a powerful mechanism responsible for the ejection of V-type asteroids into near-Earth orbits (also called as Near Earth Asteroids or NEA) and for the delivery of HED meteorites. Currently, there are some known V-type asteroids residing in near-Earth orbits, such as the following examples: (3908) Nyx, (4055) Magellan, (5604) 1992 FE or (6613) 1993 VW.

We aim to infer the mineralogical compositions of HED meteorites and of some V-type asteroids using the Hapke radiative transfer model. It is also foreseen to test the genetic linkages between V-type asteroids and HED meteorites, which was recently questioned by some authors (Schiller et al., 2011; Wasson, 2013). The paper is organized as follows: in Section 2, we describe the application of adapted Hapke's bidirectional reflectance model to the spectral deconvolution of the selected asteroids and meteorites; in Section 3, we justify the model parameterization and provide a basic description of the data selected; in Section 4, we discuss the performance of the described model on laboratorial samples, HED meteorites and V-type asteroids, we report an analysis of their mineralogies and we discuss the genetic relationship between V-type asteroids and HED meteorites; in Section 5, we stress out the outlines of this paper.

2. Model description

According to Hapke's radiative transfer model (Hapke, 1993), the bidirectional radiance coefficient (defined as the ratio of bidirectional reflectance of a surface to that of a Lambertian surface with no preferential escape of singly scattered light) of a semi-infinite medium of regolith particles whose size is larger than the wavelength λ, is given by:

$$r_H(e,i,g)=\frac{w}{4(\mu+\mu_0)}\left[[1+B_S(g)]p(g)+H(x=\mu_0,w)H(x=\mu,w)-1\right] \quad (1)$$

where i, e and g are the incidence, emergence, and phase angles, respectively, and $\mu_0=\cos(i)$, $\mu=\cos(e)$. In addition, w represents the average particle single scattering albedo, $B_S(g)$ represents the opposition effect, $p(g)$ is the average single-particle phase function, and $H(x,w)$ is the Ambartsumian–Chandrasekhar scattering function for isotropic particles. According to Mustard and Pieters (1989), $B_S(g)$ can be neglected for phase angles greater than 15°. All spectral data selected from the RELAB database satisfy this condition. The single-particle phase function is given by a two-term Legendre polynomial of the form:

$$p(g)=1+b\ \cos(g)+c\left(1.5\cos^2(g)-0.5\right) \quad (2)$$

where b describes the angular width of the scattering lobes and c describes the amplitude of the backscattered lobe relative to the forward scattered lobe. Appropriate average values for b and c were taken from Mustard and Pieters (1989) and Lucey (1998).

The Ambartsumian–Chandrasekhar function $H(x)$ is given, in very good approximation, by (Hapke, 1993):

$$H(x)=\left[1-\left[1-\sqrt{1-w}\right]x\left[r_0+\left(1-\frac{1}{2}r_0-r_0x\right)ln\left(\frac{1+x}{x}\right)\right]\right]^{-1} \quad (3)$$

where

$$r_0=\left(2/1+\sqrt{1-w}\right)-1.$$

Albedo spectra $w(\lambda)$ of minerals can be obtained from their reflectance spectra by iterative inversion of Eq. (1), provided that the corresponding phase functions are specified. Asteroid regolith's and powder mineral or meteorite analogue samples can be described as intimate mixtures of minerals for which, according to Hapke mixing model (Hapke, 1993), the average albedo (w_{mix}) is a linear combination of the albedos ($w_i; i=1,\ \ldots,\ n_m$) of the component minerals weighted by corresponding relative cross-sections (x_i):

$$w_{\mathrm{mix}}=\sum_{i=1}^{n_m}x_iw_i \quad (4)$$

The phase function of an intimate mixture is an average of the phase functions (p_i) of component minerals weighted by the products of their relative cross-sections and albedos:

$$p_{\mathrm{mix}}=\frac{\sum_{i=1}^{n_m}x_iw_ip_i}{\sum_{i=1}^{n_m}x_iw_i} \quad (5)$$

It turns out from Eq. (5) that the wavelength dependence of albedos $w_i(\lambda)$ gives rise to a wavelength dependent average phase function $p_{\mathrm{mix}}(\lambda)$, even if the phase functions $p_i(g)$ are independent of wavelength. This last assumption is valid only as an approximation, since, in general, phase functions depend on refraction index which is a function of wavelength. This means that assuming wavelength-independent phase functions for component minerals can lead to distortions in the determination of their albedos $w_i(\lambda)$. It is also known that space weathering effects have a redning effect on asteroid albedos that cannot be reproduced by albedos of intimate mixtures of pristine minerals. To account for these unavoidable modeling deficiencies, we consider an additional wavelength-dependent contribution $U(\lambda)$ to $w_{\mathrm{mix}}(\lambda)$:

$$w_{\mathrm{mix}}=\sum_{i=1}^{n_m}x_iw_i+U(\lambda) \quad (6)$$

We assume that $U(\lambda)$ is a smooth function that can be represented by a low order polynomial:

$$U(\lambda)=\sum_{k=0}^{n}A_k\lambda^k \quad (7)$$

where A_k are constant values to be fitted. This term can also model the presence of optically neutral phases not considered in the mixture. We have considered a third degree polynomial ($n=3$) in our calculations. The model radiance coefficient of a mixture of previously selected minerals, r_{mix}, is fitted to real spectra through a nonlinear least-squares minimization that takes as parameters mineral relative cross-sections (x_i) and the polynomial coefficients of function $U(\lambda)$. The goodness-of-fit is specified by the standard

deviation $\sigma_f = \sqrt{S/(N-p)}$, where S is sum of the squares of the fit residuals, N is the number of points of the fitted spectrum and $p = n_m + 3$ is the number of fitting parameters. The calculations were implemented in Microsoft Excel, using the generalized reduced gradient (GRG) nonlinear minimization method available in the Solver add-in. The relative cross-sections x_i were subject to the following constraints: $x_i \geq 0$ and $\sum_{i=1}^{n_m} x_i = 1$. Mass fractions (M_i) of component minerals are then determined through the relation:

$$M_i = \frac{\rho_i d_i x_i}{\sum_{k=1}^{n_m} \rho_k d_k x_k} \quad (8)$$

where ρ_i and d_i are, respectively, the particle density and grain size of each component mineral.

The reflectance spectra of asteroids, as measured, is often uncalibrated and normalized to unit at a given wavelength. Therefore, we adopted the usual calibration procedure by using the known value of the respective geometric albedo, which is expected to match the reflectance at $\lambda = 0.55$ μm, to unnormalize the reflectance. To derive the uncertainties in the inferred mineralogies of the asteroids, we have followed the procedure adopted by Clark et al. (2006).

3. Asteroid, meteorite and mineral selection

For the purpose of this study, we selected a set of 11 V-type asteroids from the "The MIT-UH-IRTF Joint Campaign for NEO Spectral Reconnaissance" (Rayner et al., 2003), available online at http://smass.mit.edu/minus.html. This is an ongoing joint observing program for routine measurement of Near Earth Objects (NEO) spectra, conducted by MIT, University of Hawaii and the NASA Infrared Telescope Facility (IRTF). A low-to-medium resolution NIR spectrograph and imager called SpeX, is used to obtain 0.8 to 2.5 μm spectra of NEOs. When available, visible wavelength data from SMASS survey are also included. Spectra are normalized at 0.55 μm, when visible wavelength data are available; otherwise, normalization is made near 1.21 μm. The selected set of V-type asteroids is listed in Table 1.

On the other hand, we have selected a set of 55 HED meteorites from the RELAB database (Reflectance Experiment Laboratory) (Pieters and Hiroi, 2004), available at http://www.planetary.brown.edu/relab). The laboratorial spectra were obtained in the range between 0.3 and 2.6 μm, with a sampling resolution of 0.005 μm. The RELAB instrument is designed to simulate the diverse viewing geometries in remote telescopic measurements. A 30° incident angle and a 0° emission angle (measured from the vertical) were the default parameters for the measured spectra. Further details about the RELAB database and of how the reflectance spectra were obtained are available in the RELAB user's manual. The selected set of HED meteorites is listed in Table 2.

It has long been known that the reflectance spectra of the so-called Vestoids are similar to that of (4) Vesta (McCord et al., 1970). The reflectance spectra of V-type asteroids in the visible and NIR are similar to the reflectance spectra of basaltic achondrite HED meteorites (e.g., Burbine et al., 2002). Their reflectance spectra show clearly the presence of two distinct absorption features, located at around ~0.9 and ~1.9 μm, which are indicative of the presence of pyroxene and possibly olivine minerals. In addition, the visible region of the V-type asteroids reflectance spectra shows a strong UV absorption edge also found among the HED meteorites reflectance spectra. In some cases, another observable feature is a spectral slope between 1.1 and 1.5 μm, which can be indicative of the presence of neutral phases, NiFe metal content and olivine abundance.

Table 1
List of the 11 selected V-type asteroids and related data. It is provided the type (according to the Tholen classification), some orbital elements (such as, the semi-major axis a, the eccentricity ε and the orbital period) and some physical elements (such as the diameter of the asteroids, the geometric albedo and the absolute magnitude) for each asteroid. Almost all of the data were obtained from the JPL Small-Body Database, provided by NASA, available at http://ssd.jpl.nasa.gov/sbdb.cgi#top.

Asteroid name	a (AU)	e	Diameter (km)	Geometric albedo
(4) Vesta	2.362	0.089	530.00	0.4228
(854) Frostia	2.369	0.174	7.84[2]	0.4154[2]
(3908) Nyx	1.927	0.459	1.00	0.2300
(4055) Magellan	1.820	0.326	2.49	0.3100
(5604) 1992 FE	0.927	0.405	0.55	0.4800
(6611) 1993 VW	1,696	0.484	1.20	0.3000[1]
(21238) Panarea	2.542	0.107	5.22[2]	0.3729[2]
(52750) 1998 KK17	1.427	0.525	1.06[2]	0.3930[2]
(137924) 2000 BD19	0.876	0.895	0.97[2]	0.2470[2]
(286458) 2005 VW	2.775	0.032	–	–
2003 FT3	2.673	0.572	–	–

Notes: Data obtained from: [1] Binzel et al. (2001); [2] MP^{3}C: Minor Planet Physical Properties Catalogue (available online at http://mp3c.oca.eu/MP3C/).

Pyroxenes spectra show two distinctive absorption features, located at around 1- and 2-μm (Burns, 1993), due to electronic transitions of Fe^{2+} ions in the M2 crystallographic site (Burns, 1970). According to mineral chemistry, the band centers of these two absorption features can occur at different wavelengths (Cloutis and Gaffey, 1992). Additional features near 1.2 μm can be originated by the presence of Fe^{2+} ions in the M1 site (Klima et al., 2007).

Olivines show a complex absorption at ~1 μm (Nelson et al., 1993) due to electronic transitions of Fe^{2+} in the olivine crystallographic site (Burns, 1970). This absorption feature can move towards higher wavelengths as the Fe^{2+} content increases. On the other hand, the reflectance spectrum of plagioclase shows a weak absorption peak at ~1.25 μm, which may be difficult to detect (Nelson et al., 1993).

Neutral phases are usually chosen to account for inappropriate end-member grain sizes. These minerals do not show any absorption feature as a function of the wavelength (Nelson et al., 1993). Usually, their presence is identified by an overall lowering of the albedo or by the presence of a spectral slope (Nelson et al., 1993). Actually, inferring about which opaque minerals may be present in a certain reflectance spectrum is an arduous task to accomplish. These effects can be modeled, at least partially, with the inclusion of the $U(\lambda)$ function, which may be viewed, in this context, also as an albedo background curve.

To model the mineralogies of the asteroids and meteorites considered for this study, we selected a set of reasonable end-member minerals, with appropriate grain sizes, from the RELAB database (Pieters and Hiroi, 2004). This selection took into account the possible mineralogy pointed out above for the selected V-type asteroids and HED meteorites. Hence, several types of pyroxenes, two types of olivines and plagioclases and some opaque minerals were selected (see list in Table 3).

4. Discussion

4.1. Model performance on laboratorial mixtures

To evaluate the performance of the model described in Section 2, we have first tested it in laboratorial mixtures of orthopyroxenes (Opx) and clinopyroxenes (Cpx) previously studied by Sunshine et al. (1990) and whose spectra are available in the RELAB database (Pieters and Hiroi, 2004). The samples have two distinct grain

Table 2
List of the 58 HED meteorites selected for this study. All the data were obtained from the RELAB database, publically available at http://www.planetary.brown.edu/relab.

Relab file	Sample ID	Sample name	Meteorite type	Grain size proportion	
				Min. size	Max. size
CAMP71	MP-TXH-071-A	ALHA77256,143	Diogenite	0	25
CAMP77	MP-TXH-077-A	LAP91900,27	Diogenite	0	25
CAMP95	MP-TXH-095-A	A-881526,90	Diogenite	0	25
CAMP81	MP-TXH-081-A	Aioun el Atrouss	Diogenite	0	25
CAMP88	MP-TXH-088-A	Tatahouine	Diogenite	0	25
CAMP68	MP-TXH-068-A	GRO95555,22	Diogenite	0	25
CBMB74	MB-TXH-074-A	Y-75032,HR	Diogenite	0	25
CBMB73	MB-TXH-073-A	Y-74013,HR	Diogenite	0	25
CBMB95	MB-TXH-095-B	Johnstown	Diogenite	25	45
CDMB67	MB-TXH-067-D	EETA79002,146	Diogenite	75	125
CAMP84	MP-TXH-084-A	Cachari	Eucrite	0	25
CAMP86	MP-TXH-086-A	Moore County	Eucrite	0	25
CAMB97	MB-TXH-097-A	Stannern	Eucrite	0	25
CAMP87	MP-TXH-087-A	Pasamonte	Eucrite	0	25
CBMB69	MB-TXH-069-B	Millbillillie 25–45 μm	Eucrite	25	45
CDMB96	MB-TXH-096-D	Padvarninkai	Eucrite	25	45
CCMB71	MB-TXH-071-C	Y-74450,92	Eucrite	45	75
CCMB72	MB-TXH-072-C	ALH-78132,61	Eucrite	45	75
CDMB70	MB-TXH-070-D	Juvinas	Eucrite	75	125
CDMB66	MB-TXH-066-D	ALHA76005,85	Eucrite	75	125
CDMB99	MB-TXH-099-D	ALH85001,29 <25 μm (dry-sieved)	Eucrite	0	25
CAMP89	MP-TXH-089-A	Bereba	Eucrite	0	25
CAMP90	MP-TXH-090-A	Bouvante	Eucrite	0	25
CAMP91	MP-TXH-091-A	Jonzac	Eucrite	0	25
CAMP92	MP-TXH-092-A	Serra de Mage	Eucrite	0	25
C1MT28	MT-HYM-028	MAC02522,7 eucrite	Eucrite	0	45
C1MT29	MT-HYM-029	EET87520,23 eucrite	Eucrite	0	45
C1MT30	MT-HYM-030	ALHA81001,43 eucrite	Eucrite	0	45
C1MT31	MT-HYM-031	PCA91078,16 eucrite	Eucrite	0	45
C1MT32	MT-HYM-032	BTN00300,21 eucrite	Eucrite	0	45
C1MT33	MT-HYM-033	MET01081,12 eucrite	Eucrite	0	45
CAMP96	MP-TXH-096-A	A-881819,110	Eucrite	0	25
CAMP75	MP-TXH-075-A	EET87542,25	Eucrite	0	25
C1MP118	MP-TXH-118	EET92003,15 (eucrite) <125 μm	Eucrite	0	125
C1MP119	MP-TXH-119	PCA91006,18 (eucrite) <125 μm	Eucrite	0	125
CAMP94	MP-TXH-094-A	A-87272,96	Eucrite	0	25
CAMP72	MP-TXH-072-A	EETA79005,99	Eucrite	0	25
CAMP78	MP-TXH-078-A	LEW85303,98	Eucrite	0	25
C1MP121	MP-TXH-121	ALHA81001,41 (eucrite) <125 μm	Eucrite	0	125
CAMP54	MP-TXH-054-A	Ibitira <25 μm	Eucrite	0	25
CAMP73	MP-TXH-073-A	EET83376,12	Howardite	0	25
CAMP98	MP-TXH-098-A	Y-790727,144	Howardite	0	25
CAMP99	MP-TXH-099-A	Y-791573,145	Howardite	0	25
C1MP125	MP-TXH-125	GRO95574,9 (howardite) <125 μm	Howardite	0	125
C1MP126	MP-TXH-126	QUE97001,28 (howardite) <125 μm	Howardite	0	125
C1TB127	TB-TJM-127	Bialystok	Howardite	0	150
CAMP70	MP-TXH-070-A	Petersburg	Howardite	0	25
CAMP97	MP-TXH-097-A	Y-7308,142	Howardite	0	25
CAMP67	MP-TXH-067-A	GRO95535,12	Howardite	0	25
CAMP82	MP-TXH-082-A	Binda	Howardite	0	25
CAMP83	MP-TXH-083-A	Bununu	Howardite	0	25
CAMP85	MP-TXH-085-A	Frankfort howardite	Howardite	0	25
CAMP93	MP-TXH-093-A	Le Teilleul	Howardite	0	25
CAMP53	MP-TXH-053-A	Kapoeta	Howardite	0	25
CAMP69	MP-TXH-069-A	QUE94200,19	Howardite	0	25
CDMB68	MB-TXH-068-D	EET87503,97 75–125 μm	Howardite	75	125

sizes: small (<45 μm) and large (70–145 μm). The chosen end-member minerals, with appropriated grain sizes, were also obtained from the RELAB database. One can observe that the mineralogies obtained for these Opx–Cpx samples, as listed in Table 4, agree with the ones of Sunshine et al. (1990) within a margin error of 5% for grain sizes <45 μm and 70–145 μm. A better agreement would be possible if the grain size (70–125 μm) of the chosen end-member minerals matched the grain size of the analyzed mixtures, since it is known that spectral absorption features are strongly affected by grain size effects (see e.g. Hapke, 1993 and references therein). In general, absorption increases with grain size leading to more pronounced absorption peaks in reflectance spectra. Indeed, the RELAB database does not include any Cpx or Opx spectra corresponding to grain sizes larger than 125 μm that could be used to avoid this problem.

4.2. Model performance on HED meteorites

We have initially analyzed the effect of grain size on the determination of the mineralogy of the same meteorite. For this purpose, we considered the following RELAB samples of the meteorite Y-74450 with different grain size ranges (GSR): MB-TXH-071-A (GSR: 0–25 μm; sample A); MB-TXH-071-B (GSR: 25–45 μm; sample B);

Table 3
List of the end-member minerals selected for this study. All the table content and data were obtained from the RELAB database, publically available at http://www.planetary.brown.edu/relab.

Relab file	Sample ID	Sample name (RELAB)	Mineral subtype (RELAB)	Grain size proportion	
				Min. size	Max. size
CAPP37	PP-TXH-037-A	Seven Sisters Is.	Plagioclase	0	25
C1PP46	PP-EAC-046	PYX015	Pyroxene Endiopside[a]	0	45
C1PP21	PP-CMP-021	Cpx 45	Pyroxene clinopyroxene diopside	0	45
CAPP38	PP-TXH-038-A	St. Ludger-de-Milot hypersthene <25 μm	Hypersthene	0	25
CAPA60	PA-CMP-060-A	Split rock anorthite	Anorthite	0	25
C1DL08A	DL-CMP-008-A	Wo 5 En 38 Fs 57 (E36-103, 100% opx) <45 μm	Pyroxene clinopyroxene pigeonite	0	45
C1AG10	AG-TJM-010	Augite	Pyroxene clinopyroxene augite	0	45
C1DD98	DD-MDD-098	Fa 100 Fo 0 <45 μm	Olivine fayalite	0	45
C1DD85P	DD-MDD-085-P	Fa 0 Fo 100 <45 μm pellet	Olivine forsterite	0	45
CACR11	CR-EAC-011	CHR101	Chromite	0	45
C1PE30	PE-CMP-030	Web 45	Enstatite	0	45
CJB236	JB-JLB-236	NMNH-120414-1	Pyroxene orthopyroxene bronzite	0	45
CAEA09	EA-EAC-009-A	TRO203A	Troilite	0	45
CBPP37	PP-TXH-037-B	Seven Sisters Is.	Plagioclase	25	45
CBPP38	PP-TXH-038-B	St. Ludger-de-Milot hypersthene 25–45 μm	Hypersthene	25	45
CBPA60	PA-CMP-060-B	Split rock anorthite	Anorthite	25	45
CCPP37	PP-TXH-037-C	Seven Sisters Is.	Plagioclase	45	75
C1PP01	PP-EAC-001	PYX005	Pyroxene clinopyroxene Endiopside[a]	45	90
C1PP22	PP-CMP-022	Cpx 75	Pyroxene clinopyroxene diopside	45	75
CCPP38	PP-TXH-038-C	St. Ludger-de-Milot hypersthene 45–75 μm	Hypersthene	45	75
C1PA60	PA-CMP-060-C	Split Rock Anorthite	Anorthite	45	75
C1LR180	LR-CMP-180	70035,188 light-brown pyroxene B	Pyroxene clinopyroxene pigeonite	0	125
C1PO71	PO-CMP-071	St. Peter's fayalite	Olivine fayalite	45	75
C1PO77	PO-CMP-077	Apache forsterite	Olivine forsterite	45	75
C1PE31	PE-CMP-031	Web 75	Enstatite	45	75
C1PP52	PP-EAC-052	PYX119	Pyroxene orthopyroxene bronzite	45	90
C1MB06	MB-CMP-006	Mundrabilla troilite	Troilite	0	250
C1SR70A	SR-JFM-070-A	BUR-5080	Pyroxenoid wollastonite	45	150
CDPP37	PP-TXH-037-D	Seven Sisters Is.	Plagioclase	75	125
C1PP23	PP-CMP-023	Cpx 125	Pyroxene clinopyroxene diopside	75	125
CDPP38	PP-TXH-038-D	St. Ludger-de-Milot hypersthene 75–125 μm	Hypersthene	75	125
CDPA60	PA-CMP-060-D	Split Rock Anorthite	Anorthite	75	125
C1SR43A	SR-JFM-043-A	AZ-01	Olivine forsterite	45	150
C1PE32	PE-CMP-032	Web 125	Enstatite	75	125
C1LR78	LR-CMP-178	70017,535 ilmenite	Ilmenite	0	125
CASP16	SP-EAC-016	SPI116	Spinel	0	45

[a] *Endiopside* is an obsolete term referring to magnesium-rich (or Mg-rich) augite. See Morimoto et al. (1989) for more details.

Table 4
Results of spectral deconvolution of selected Cpx–Opx mixture samples. The inferred mineralogies by Sunshine et al. (1990) and the standard deviation of the fits are also listed. The selected Cpx end-members were: PP-CMP-021 (0–45 μm); PP-CMP-022 (45–75 μm); and PP-CMP-023 (75–125 μm). On the other hand, the selected Opx end-members were: PE-CMP-030 (0–45 μm); PE-CMP-0031 (45–75 μm); and PE-CMP-032 (75–125 μm).

RELAB sample ID	RELAB file	Grain size (μm)	This study		Sunsine et al. (1990)		A_0	A_1	A_2	A_3	σ
			Opx	Cpx	Opx	Cpx					
XP-CMP-010	C1XP10	0–45	49	51	50	50	0.0361	−0.0572	0.0331	−0.0063	2.10^{-3}
XP-CMP-011	C1XP11	0–45	56	44	60	40	0.0305	−0.0444	0.0252	−0.0047	3.10^{-3}
XP-CMP-012	C1XP12	0–45	37	63	40	60	0.0239	−0.0437	0.0217	−0.0034	1.10^{-3}
XP-CMP-013	C1XP13	0–45	73	27	75	25	0.0313	−0.0413	0.0204	−0.0033	1.10^{-3}
XP-CMP-014	C1XP14	0–45	20	80	25	75	0.0307	−0.0576	0.0285	−0.0046	2.10^{-3}
XP-CMP-015	C1XP15	0–45	84	16	85	15	0.0358	−0.0416	0.0239	−0.0048	2.10^{-3}
XP-CMP-016	C1XP16	0–45	17	83	15	85	0.0108	−0.0104	0.0036	−0.0006	1.10^{-3}
XP-CMP-001	C1XP01	70–145	45	55	50	50	−0.0255	−0.0014	0.0024	−0.0007	5.10^{-3}
XP-CMP-002	C1XP02	70–145	52	48	60	40	−0.0181	−0.0112	−0.0093	0.0042	7.10^{-3}
XP-CMP-003	C1XP03	70–145	35	65	40	60	−0.0348	0.0016	−0.0009	0.0004	5.10^{-3}
XP-CMP-004	C1XP04	70–145	74	26	75	25	−0.0266	−0.0142	−0.0014	0.0016	4.10^{-3}
XP-CMP-005	C1XP05	70–145	21	79	25	75	0.0091	−0.1174	0.0713	−0.0140	4.10^{-3}
XP-CMP-006	C1XP06	70–145	83	17	85	15	0.0247	−0.0505	0.0136	−0.0006	4.10^{-3}
XP-CMP-007	C1XP07	70–145	11	89	15	85	−0.0646	0.0072	−0.0180	0.0049	3.10^{-3}

MB-TXH-071-C (GSR: 45–75 μm; sample C); and MB-TXH-071-D (GSR: 75–125 μm; sample D).

One can see from Fig. 1 that, because of increasing bulk absorption, the reflectance of these samples is reduced globally with increasing grain size. The reduction in reflectance is more pronounced from 0–25 μm to 25–45 μm grain size ranges resulting in that spectral differences among samples B, C and D are significantly smaller than those between samples A and B. The inferred mineralogies for all Y-74450 samples are listed in Table 5 and the corresponding fits are shown in Fig. 2. Mineralogies of

samples B, C and D deviate less than 5% from their average value, but this differs in 10–15% from the mineralogy of sample A, with larger differences in Opx, Cpx and chromite abundances.

To deeper analyse the impact of uneven spectral changes induced by grain size variation, we list the detailed inferred mineralogical composition of samples A and B in Table 6. It is clear that the mixing model inferred for sample A, which has the largest reflectance, the presence of high reflectance minerals (wollastonite, forsterite and plagioclase) in detriment of diogenite, hypersthene, piogenite and chromite, which are enriched in the composition of sample B. In sample A, the abundances of the latter minerals appear to have been transferred partially to other minerals that have similar absorption features. In general, the transfer of abundance of one mineral to another one can occur without any significant fit improvement when their reflectance spectra show important similarities (e.g., spectral bands in the case of the pyroxenes). Despite the differences between the inferred abundances of Opx and Cpx for these four samples, it is important to stress out that the total pyroxene abundance (Opx+Cpx) is approximately equal in all of them: 65% in sample A; 66% in samples B and D; 68% in sample-C. It is likely that the spurious disparities in the inferred mineralogies of samples A–D are caused by grain size effects unaccounted for by the mixing model as, e.g., the intrinsic dependence of the phase function parameters b and c on grain size.

The mixing model was also applied to the HED meteorites listed in Table 2, to infer about their mineralogical compositions. We list the inferred mineralogies for all HED meteorites in Table 7. The goodness of the fits for the results listed in Table 7 ranges between 2.2×10^{-3} (for the best fit) and 1.3×10^{-2} (for the worst fit). In Fig. 3, we show the boxplots of the derived abundances of Opx and Cpx for the selected HED meteorites. The average mineralogical composition for the selected eucrites is $21 \pm 3\%$ of orthopyroxenes, $40 \pm 4\%$ of clinopyroxenes, $10 \pm 3\%$ of olivine, $7 \pm 2\%$ of chromite, $11 \pm 3\%$ of troilite, $6 \pm 1\%$ of spinel and $3 \pm 1\%$ of plagioclase. On the other hand, the average mineralogical composition for the selected howardites is $47 \pm 7\%$ of orthopyroxenes, $25 \pm 4\%$ of clinopyroxenes, $8 \pm 3\%$ of olivine, $5 \pm 2\%$ of chromite, $7 \pm 3\%$ of troilite and $6 \pm 1\%$ of spinel. The average mineralogical composition of the ten diogenites samples is $73 \pm 10\%$ of orthopyroxenes, $13 \pm 2\%$ of clinopyroxenes, $5 \pm 1\%$ of olivine, $5 \pm 2\%$ of chromite, $2 \pm 2\%$ of troilite and $2 \pm 1\%$ of spinel.

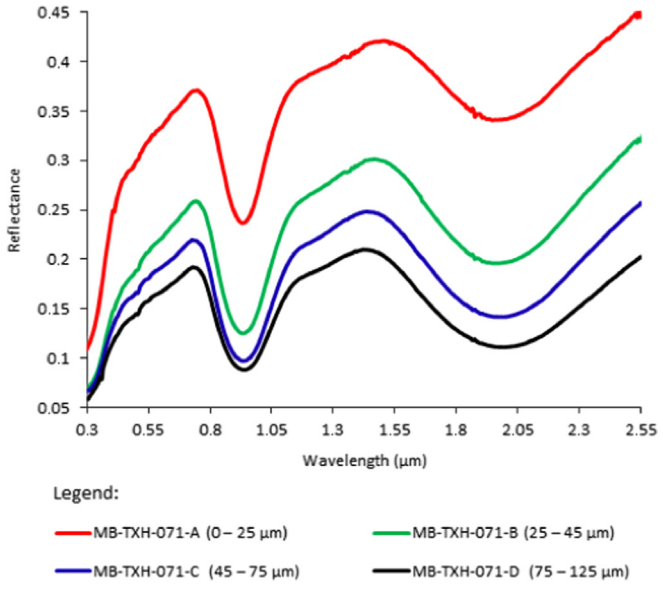

Fig. 1. Reflectance spectra of the samples MB-TXH-071-A, MB-TXH-071-B, MB-TXH-071-C and MB-TXH-071-D of meteorite Y-74450.

Bowman et al. (1997) derived the average mineralogical composition for 21 diogenites and reported that these samples were composed by 92.2% of orthopyroxenes, 4.2% of olivine, 1.2% of clinopyroxenes, 0.9% of spinel, 0.4% of plagioclase, 0.1% of FeNi metal, 0.6% of troilite and 0.4% of silica phase. The average values that we derived for orthopyroxenes and clinopyroxenes do not seem to agree with the ones derived by Bowman et al. (1997), but our sample of diogenites represents just a subset of the sample used by Bowman et al. (1997). It is also possible that when, as in this case, fits involve a mineral mixture with more than two end-members, the uncertainty in the mineralogy determination may be larger than the uncertainty of 5% estimated for binary mixtures in Section 4.1. Despite the average values seem to disagree, we found that, on average, orthopyroxenes are clearly a major component of diogenites, as stressed out by Bowman et al. (1997). We have also detected the presence of olivine.

We have also compared some of our fitting results to the mineralogies inferred by other authors. Initially, we will consider the three following diogenitic samples: MP-TXH-068-A (GRO95555, henceforth GRO), MB-TXH-081-A (Aioun el Atrouss), and MB-TXH-095-B (Johnstown). For each of these samples, we made ten fits with different initial conditions. We have noticed that the mixing model described in Section 2 is independent of the initial guessed modal composition and will converge, on average, to the same final solution. The results of corresponding best fit for each meteorite is shown in Fig. 4 and the inferred mineralogy is listed in Table 8. In all three cases, the background curve is nonmonotonic. Despite the fits are globally satisfactory, both qualitatively and quantitatively, they are clearly unable to fully reproduce a few spectral features. As examples, one can observe the misfit 1.3 μm for GRO, or the observed misfit 0.6–0.8 μm for Aioun el Atrouss. This misfit may be caused by different grain sizes of the meteorite samples and the assumed component minerals whose spectra were selected for spectral mixing.

We will also compare our individual results for these three diogenites with other studies in the literature. In this analysis, we will consider that our results are in good agreement with other authors if the differences are inferior than 5%. Hereafter, we will discuss on the individual cases:

MP-TXH-068-A (*GRO*): Papike et al. (2000) inferred that GRO is composed by 96.7% of orthopyroxenes, 1.5% of spinel, 1.4% of silica phase and 0.2% of troilite and FeNi metal. We have found a lower orthopyroxene content (85%) than Papike et al. (2000). We have also found the presence of clynopiroxenes, in contrast to the

Table 5
Inferred mineralogies for the samples of Y-74450 (see text for more details). The values are listed in units of vol%.

Sample	Opx	Cpx	Olivine	Anorthite	Chromite	Spinel	Opx+Cpx	σ
MB-TXH-071-A	49	16	19	4	–	12	65	4.4×10^{-3}
MB-TXH-071-B	31	35	15	–	10	9	66	5.8×10^{-3}
MB-TXH-071-C	37	31	11	–	12	9	68	5.5×10^{-3}
MB-TXH-071-D	40	26	11	–	15	8	66	4.7×10^{-3}
Average	39	27	14	1	9	10	66	–

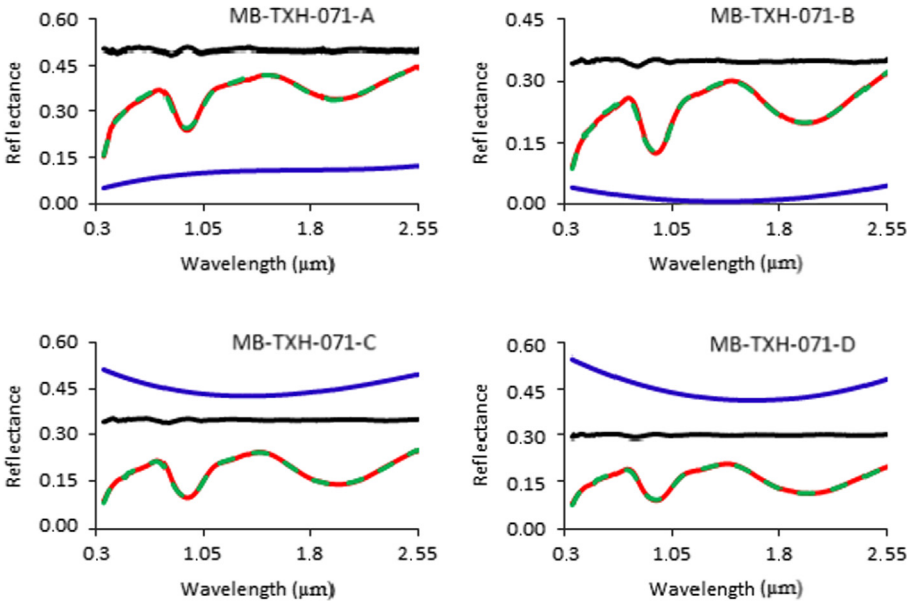

Fig. 2. Fit modeled curve (green dashed line) of the reflectance spectra (red line) of the four samples of Y-74450. Fit residuals (black line) were vertically shifted by: 0.50 units for MB-TXH-071-A; 0.35 units for MB-TXH-071-B and MB-TXH-071-C; 0.30 units for MB-TXH-071-D. The $U(\lambda)$ curves (blue line) were vertically shifted by: 0.15 units for MB-TXH-071-A; 0.50 units for MB-TXH-071-C; 0.55 units for MB-TXH-071-D. The $U(\lambda)$ curve was not shifted for MB-TXH-071-B. *Top left:* Plot for MB-TXH-071-A. *Top right:* Plot for MB-TXH-071-B. *Bottom left:* Plot for MB-TXH-071-C. *Bottom right:* Plot for MB-TXH-071-D. (For interpretation of the references to color in this figure legend, the reader is referred to the web version of this article.)

Table 6
Detailed mineralogy inferred for samples MB-TXH-071-A and MB-TXH-071-B. The values are listed in units of vol%.

Sample ID	Plag	Dio	Hyper	Aug	Pio	Bron	Enst	Wolla	Fors	Faya	Chro	Spi
MB-TXH-071-A	4	–	12	8	13	10	4	18	9	11	–	12
MB-TXH-071-B	–	12	35	–	19	–	–	–	–	15	10	9

Legend: Plag.: Plagioclase; Dio: Diopside; Hyper: Hypersthene; Aug: Augite; Pio: Pigeonite; Faya: Fayalite; Fors: Forsterite; Chro: Chromite; Enst: Enstatite; Bron: Bronzite; Wolla: Wollastonite; Spi: Spinel.

results of Papike et al. (2000). We have not found traces of neutral phases, which is in agreement with the low abundance of neutral phases found by Papike et al. (2000).

MP-TXH-081-A (*Aioun el Atrouss*): The inferred orthopyroxene (77%) abundance is lower than the one found by Bowman et al. (1997) (98%, on average). We have found the presence of clinopyroxenes and a higher average content of chromite than Bowman et al. (1997).

MB-TXH-095-B (*Johnstown*): Zema et al. (1997) inferred an average enstatite, ferrosilite and wollastonite content of 73.7%, 23.5% and 2.8%, respectively. We have found a lower enstatite content for Johnstown than Zema et al. (1997) and Bowman et al. (1997). On the other hand, we have not found the presence of wollastonite. The latter is in agreement with Bowman et al. (1997), but opposing to the value reported by Zema et al. (1997). Bowman et al. (1997) found some traces of olivine on Johnstown, while we have found an olivine content of 10%. We have not found traces of troilite, while Bowman et al. (1997) inferred a presence of 2%. Donaldson and Sprague (2009) used a spectral deconvolution method to infer the following mineralogical composition for Johnstown: 66–76% of hypersthene; 21–31% of diopside; 5–15% of anorthite; 3–13% of olivine; and 0–10% of chromite. Our results are in good agreement with Donaldson and Sprague (2009). The average orthopyroxene content inferred here is around 50%, being lower than the range presented by Donaldson and Sprague (2009). The inferred average clinopyroxenes abundance is higher than the range of Donaldson and Sprague (2009). On the other hand, the average olivine content is within the range given by Donaldson and Sprague (2009). We have not found, however, the presence of anorthite. Lawrence and Lucey (2007) have modeled the spectrum of Jonhstown using the Hapke radiative transfer model and have obtained the following modal mineralogy: 4.6% of olivine; 91.0% of orthopyroxenes; 5.2% of clinopyroxenes; 3.6% of plagioclase feldspar; 2.9% of troilite; 3.8% of glass; and 3.4% of Fe–Ni metal. Indeed, we have also inferred that orthopyroxenes have the highest modal content, but our value is lower than the one obtained by Lawrence and Lucey (2007). On the other hand, we have found a higher modal content of clinopyroxenes and a content of neutral phases higher than Lawrence and Lucey (2007) and no traces of olivine. Our modeled curve for the Johnstown meteorite (see Fig. 4) seems to better reproduce the experimental curve than the one presented by Lawrence and Lucey (2007).

We have also considered the average mineralogy listed in Table 5 for the polymict eucrite Y-74450, to compare against other studies. Lawrence and Lucey (2007) have performed a mixing spectral analysis of this meteorite and have inferred the following modal mineralogy: 4.6% of olivine, 30.5% of orthopyroxenes, 21.3% of clinopyroxenes, 36.0% of plagioclase, 1.2% of troilite and 2.1% of glass. On the other hand, Delaney et al. (1983) and Middlefehldt et al. (1998) have measured the following modal abundance for Y74450: 0.1% of olivine, 35.2% of orthopyroxene, 16.3% of clinopyroxene, 39.2% of feldspar, 0.7% of troilite and 4.8% of glass. Our inferred average abudance of orthopyroxenes is in good agreement with Delaney et al. (1983) and Middlefehldt et al. (1998), apart from a higher abundance of clinopyroxene and a lower abundance of plagioclase. Our results show, however, a higher abundance of neutral phases, such as chromite and spinel. The percentages of clinopyroxenes, orthopyroxenes and olivine are also in good agreement with Lawrence and Lucey (2007). However, our results evidence a much lower

Table 7
Inferred mineralogies of all HED meteorites listed in Table 2. The inferred mineralogy for the sample MB-TXH-071-C is already listed in Table 5. The values are listed in units of vol%.

Sample ID	Plag	End	Dio	Hyper	Anor	Aug	Pio	Faya	Fors	Chro	Enst	Hed	Bron	Troi	Wolla	Ilm	Phos	Spi
MP-TXH-071-A	–	–	–	–	–	–	7	20	–	–	22	–	51	–	–	–	–	–
MP-TXH-077-A	–	–	–	–	–	–	12	–	–	9	78	–	–	–	–	–	–	–
MP-TXH-095-A	–	–	–	12	–	–	13	10	–	–	37	–	28	–	–	–	–	–
MP-TXH-081-A	–	–	–	–	–	–	13	–	–	9	77	–	–	–	–	–	–	–
MP-TXH-088-A	–	–	–	–	–	–	13	–	–	9	77	–	–	–	–	–	–	–
MP-TXH-068-A	–	–	–	–	–	–	14	1	–	–	85	–	–	–	–	–	–	–
MB-TXH-074-B	–	–	–	6	–	–	21	–	–	–	54	–	14	–	–	3	–	2
MB-TXH-073-B	–	–	–	–	–	–	7	12	–	–	27	–	54	–	–	–	–	–
MB-TXH-095-B	–	–	–	–	–	–	15	5	–	3	72	–	–	–	–	–	–	5
MB-TXH-067-D	–	–	–	–	–	–	15	–	–	15	38	–	–	21	–	–	–	11
MP-TXH-084-A	–	–	9	–	–	–	26	20	–	–	31	–	5	–	10	–	–	–
MP-TXH-086-A	–	–	19	2	–	2	28	–	–	–	47	–	–	–	–	1	–	–
MB-TXH-097-A	–	3	–	7	–	5	17	–	–	–	9	–	–	50	–	–	–	9
MP-TXH-087-A	–	–	–	35	5	15	19	4	4	–	–	–	–	10	2	1	–	5
MB-TXH-069-B	–	–	–	–	–	10	41	–	6	13	19	–	–	–	–	–	–	11
MB-TXH-096-D	–	–	–	–	–	12	37	–	–	13	13	–	–	8	–	–	–	17
MB-TXH-072-C	–	–	–	–	–	–	40	–	–	5	14	–	–	26	–	–	–	14
MB-TXH-070-D	–	–	–	–	–	–	41	–	–	17	23	–	–	–	–	–	–	18
MB-TXH-066-D	–	–	–	–	–	11	43	–	–	46	–	–	–	–	–	–	–	–
MB-TXH-099-D	–	–	–	–	–	–	35	–	–	34	2	–	–	26	–	–	–	4
MP-TXH-089-A	–	–	–	–	–	–	10	–	6	1	36	–	–	37	–	–	–	11
MP-TXH-090-A	31	9	–	12	–	9	20	–	–	–	7	–	–	–	–	–	–	11
MP-TXH-091-A	–	–	–	–	–	15	17	–	–	9	18	–	–	26	–	–	–	15
MP-TXH-092-A	–	–	–	4	–	6	25	–	–	–	23	–	–	31	–	–	–	11
MT-HYM-028	–	–	–	–	–	–	11	–	38	1	23	–	–	20	–	–	–	7
MT-HYM-029	–	–	–	–	–	64	27	9	–	–	–	–	–	–	–	–	–	–
MT-HYM-030	–	–	–	9	–	39	27	–	–	–	18	–	–	–	–	2	–	5
MT-HYM-031	–	–	–	–	–	–	14	–	56	–	13	–	–	–	–	–	–	18
MT-HYM-032	–	–	–	–	–	27	29	–	–	30	1	–	–	12	–	–	–	1
MT-HYM-033	–	–	–	–	–	–	49	13	–	4	5	–	–	24	–	5	–	–
MP-TXH-075-A	–	–	–	–	–	7	4	19	–	–	7	–	25	38	–	–	–	–
MP-TXH-118	–	–	–	–	–	–	12	44	–	–	5	24	–	–	13	–	2	–
MP-TXH-119	–	–	–	–	–	–	–	25	–	42	17	10	–	–	7	–	–	–
MB-TXH-096-A	–	–	–	14	26	15	10	1	–	–	–	–	–	34	–	–	–	–
MP-TXH-094-A	–	24	–	10	8	12	28	–	–	–	–	–	13	–	–	–	–	6
MP-TXH-072-A	–	–	–	46	14	5	17	3	–	–	9	–	–	–	–	–	–	5
MP-TXH-078-A	–	–	–	26	14	18	18	6	–	–	–	–	10	–	–	–	–	8
MP-TXH-121	–	–	–	–	–	19	25	7	–	–	22	–	7	–	–	–	–	20
MP-TXH-054-A	–	–	–	24	–	24	24	5	–	–	21	–	–	–	–	3	–	–
MP-TXH-070-A	–	–	–	–	–	–	8	40	–	–	16	–	–	36	–	–	–	–
MP-TXH-097-A	1	–	–	–	–	10	19	–	–	–	23	–	–	–	37	–	–	10
MP-TXH-067-A	–	–	–	22	–	2	15	–	17	–	21	–	–	16	–	–	–	7
MP-TXH-082-A	–	–	–	–	–	–	25	–	–	10	65	–	–	–	–	–	–	–
MP-TXH-083-A	–	–	–	–	–	4	17	–	–	–	44	–	–	–	34	–	–	1
MP-TXH-085-A	–	–	–	–	–	–	18	–	–	9	61	–	–	7	–	–	–	5
MP-TXH-093-A	–	–	–	–	–	–	20	–	–	6	67	–	–	–	–	–	–	8
MP-TXH-069-A	–	–	–	–	–	–	12	–	–	–	63	–	–	15	–	–	–	10
MB-TXH-068-D	–	–	–	–	–	2	24	–	–	18	19	–	–	31	–	–	–	6
MP-TXH-073-A	–	–	–	46	25	3	18	1	–	–	–	–	–	–	–	–	–	6
MP-TXH-098-A	–	–	–	–	–	–	15	18	–	–	29	–	38	–	–	–	–	–
MP-TXH-099-A	–	–	–	–	–	–	10	24	–	–	35	–	31	–	–	–	–	–
MP-TXH-125	–	–	–	–	–	–	20	–	–	13	58	–	–	–	–	–	–	9
MP-TXH-126	–	–	–	–	–	7	19	–	–	6	48	–	–	6	–	–	–	14
TB-TJM-127	–	–	–	–	–	–	42	22	–	11	12	–	–	–	–	–	–	13

Legend: Plag: Plagioclase; End: Endiopside; Dio: Diopside; Hyper: Hypersthene; Anor: Anorthite; Aug: Augite; Pio: Pigeonite; Faya: Fayalite; Fors: Forsterite; Chro: Chromite; Enst: Enstatite; Hed: Hedenbergite; Bron: Bronzite; Troi: Troilite; Wolla: Wollastonite; Ilm: Ilmenite; Phos: Phosphates; Spi: Spinel.

abundance of plagioclase. One can also observe from the values listed in Table 5 that we have detected a similar percentage of anorthite only on the first sample (MB-TXH-071-A) as Lawrence and Lucey (2007).

Spectral mixing models are strongly dependent on the choice of reasonable end-member minerals. We have selected a larger number of end-member minerals to perform the spectral mixing than Lawrence and Lucey (2007). Besides the differences in the adopted fit models, this fact may explain part of the differences in the derived modal mineralogies. In addition, our modeled spectral curves of Y74450 (see Fig. 1) are a better representation of the absorption features of this meteorite, when compared to that obtained by Lawrence and Lucey (2007).

The results discussed in this section evidenced that the model described in Section 2 is able not only to provide globally satisfactory fits to HED meteoritic spectra but also mineralogical compositions which are generally in good agreement with results of other authors.

4.3. Model performance on V-type asteroids

We have performed an analysis to test the strength of our model solution. For this purpose, we have considered the fit of

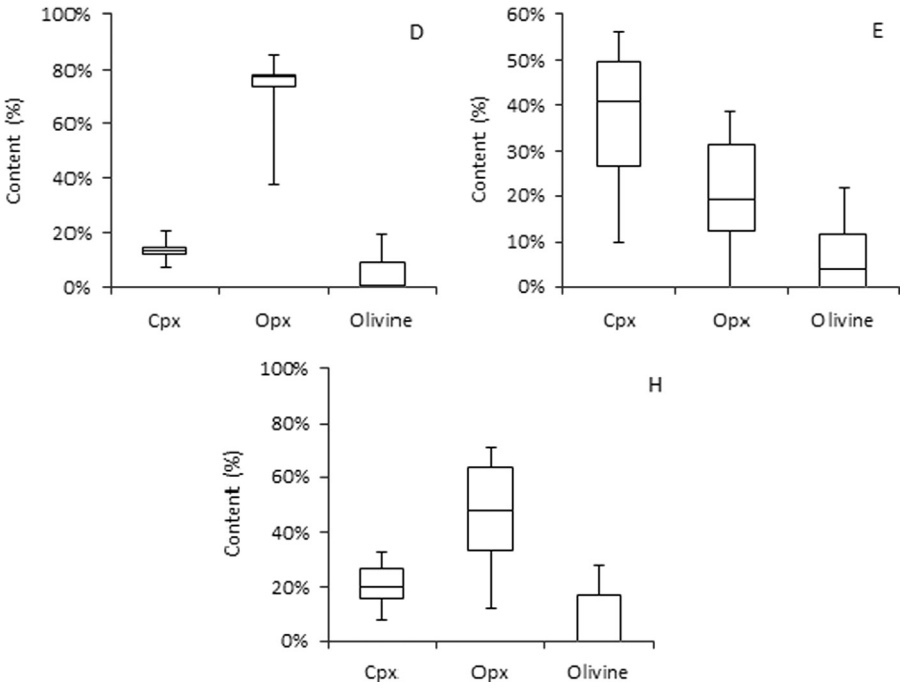

Fig. 3. Boxplots of the derived clinopyroxenes (Cpx) and orthopyroxenes (Opx) assemblages for the selected diogenites D (top left), eucrites E (top right) and howardites H (bottom), listed in Table 2.

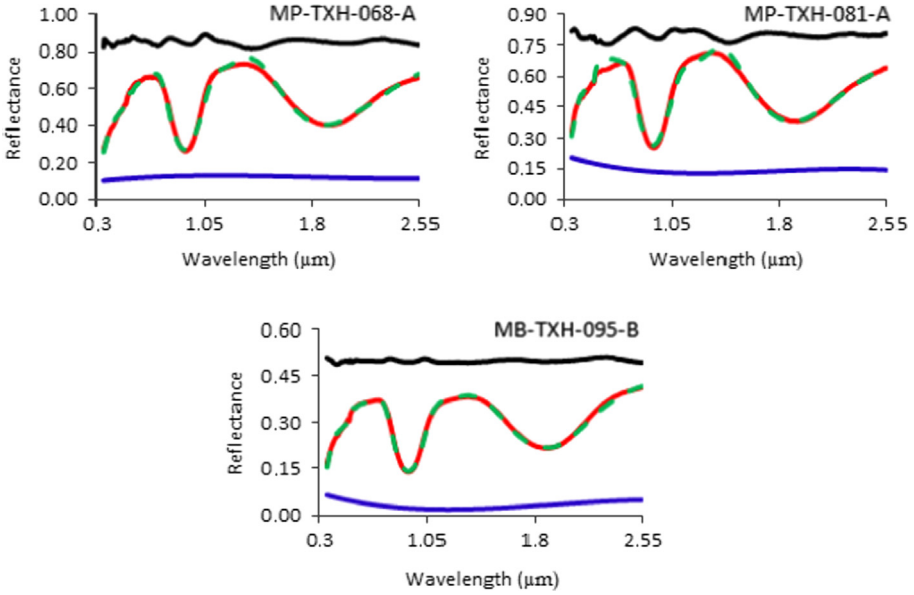

Fig. 4. Best fit model (green dashed line) of the reflectance spectra of three diogenites (red line). Fit residuals (black line) were vertically shifted by: 0.8 units for MP-TXH-068-A and MP-TXH-081-A; 0.5 units for MB-TXH-095-B. The $U(\lambda)$ curves (blue line) were vertically shifted by: 0.1 units for MB-TXH-095-B, MP-TXH-068-A and MP-TXH-081-A. *Top left:* Plot for the diogenite GRO95555 (MP-TXH-068-A), with $\sigma \sim 6 \times 10^{-3}$. *Top right:* Plot for the diogenite Aioun el Atrouss (MP-TXH-081-A), with $\sigma \sim 7 \times 10^{-3}$. *Bottom:* Plot for the diogenite Johnstown (MB-TXH-095-B), with $\sigma \sim 5 \times 10^{-3}$. (For interpretation of the references to color in this figure legend, the reader is referred to the web version of this article.)

Table 8
Average inferred mineralogies of three diogenites. The values are listed in units of vol%.

Meteorite	Hyper	Anor	Pio	Faya	Chro	Enst	Bron	Troi	Ilm	Spi	σ
MP-TXH-068-A	–	–	14	1	–	85	–	–	–	–	6.10^{-3}
MP-TXH-081-A	–	–	13	–	10	77	–	–	–	–	7.10^{-3}
MB-TXH-095-B	12	–	13	10	–	37	28	–	–	–	5.10^{-3}

Legend: Hyper: Hypersthene; Anor: Anorthite; Pio: Pigeonite; Faya: Fayalite; Chro: Chromite; Enst: Enstatite; Bron: Bronzite; Troi: Troilite; Ilm: Ilmenite; Spi: Spinel.

Table 9
Modeled surface mineralogies of asteroid (4) Vesta for the different cases (see text). The values are listed in order of decreasing σ, in units of vol%.

Case	End	Hyper	Anor	Aug	Pio	Faya	Chro	Enst	Hed	Bron	Troi	Ilm	Spi	σ
11	–	–	–	–	20	–	2	4	–	–	74	–	–	1.8×10^{-2}
6	–	–	–	25	–	16	22	23	–	–	–	–	14	8.8×10^{-3}
	–	–	58	–	27	–	–	15	–	–	–	–	–	7.5×10^{-3}
2	–	–	–	–	15	6	3	39	–	–	–	–	38	7.3×10^{-3}
9	–	27	14	5	19	1	19	–	–	6	–	10	–	3.6×10^{-3}
8	–	25	–	3	16	–	–	10	5	–	–	4	36	3.3×10^{-3}
10	–	40	–	5	15	2	9	2	3	–	–	–	25	3.1×10^{-3}
3/4/7	–	35	–	4	18	–	9	–	2	4	–	8	21	3.1×10^{-3}
1	35	–	–	–	20	–	8	–	–	5	–	14	17	2.9×10^{-3}

Legend: End: Endiopside; Hyper: Hypersthene; Anor: Anorthite; Aug: Augite; Pio: Pigeonite; Faya: Fayalite; Chro: Chromite; Enst: Enstatite; Hed: Hedenbergite; Bron: Bronzite; Troi: Troilite; Ilm: Ilmenite; Spi: Spinel.

(4) Vesta to investigate the impact on the model performance if we start to substract the presence of minerals from the fitting process. To test this scenario, we have considered the following cases in the fitting process: (1) absence of orthopyroxenes; (2) absence of clinopyroxenes; (3) absence of olivine; (4) absence of plagioclase; absence of all neutral phases; (6) absence of piogenite; (7) absence of enstatite; (8) absence of chromite; (9) absence of spinel; (10) absence of ilminite; (11) absence of the $U(\lambda)$ curve. The modeled surface mineralogies of (4) for these cases are listed in Table 9. From these results, one can observe the differences in the inferred mineralogies and how the model adapts itself for the different cases. Of key interest is to observe the importance of the presence of clinopyroxenes, piogenite, neutral phases and of the $U(\lambda)$ curve in the fitting process. The latter is evidenced by the goodness of the fits listed in Table 9. Indeed, these results are evidencing the presence of clinopyroxenes and neutral phases in the surface regolith of (4) Vesta. The method is based on a minimization procedure that tries to find the model parameters that give the best fit. Our efforts to ensure, as much as possible, global minimization allow us to consider that any results derived from the fittings depend, essentially, on the adopted model and not on the fitting process.

We have also applied the model described in Section 2 to the V-type asteroids listed in Table 1, for which we found a geometric albedo value in the literature. We list the inferred mineralogies and corresponding uncertainties, following the methodology adopted by Clark et al. (2006), in Table 10 and show the corresponding fits in Figs. 5–6. As one can observe from these figures, all modeled curves reproduce well the reflectance spectra of the asteroids. As expected, fit residuals show, in general, a flat behavior dominated by spectral noise. The exceptions is (137924) 2000 BD19, for which fit residuals show oscillations unrelated to spectral noise. For asteroids (4) Vesta, (52750) 1998 KK17 and (137924) 2000 BD19, the $U(\lambda)$ polynomials are increasing monotonous, which may be indicative of spectral reddening produced by space weathering effects on these asteroids (Clark et al., 2002). In the other cases, this cannot be ascertained because the $U(\lambda)$ polynomials show a nonmonotonous variation with wavelength.

In order to test the performance of the mixing model in V-type asteroids, we compare our inferred modal abundances with the literature (e.g., Lawrence and Lucey, 2007; Donaldson and Sprague, 2009). It is also worth to mention that the modeled surface composition of (4) Vesta is consistent with an eucritic-to-howarditic composition (see the mineralogical distributions of orthopyroxenes and clinopyroxenes for eucrites, shown in Fig. 3). The latter is also in agreement with the results from the Dawn mission (e.g., de Sanctis et al., 2013).

Lawrence and Lucey (2007) performed a mixing spectral analysis of (4) Vesta and inferred the following surface mineralogy: 38.0% of orthopyroxenes, 27.6% of clinopyroxenes, 41.0% of anorthite and 1.0% of troilite. Our analysis of (4) Vesta is based on a reflectance spectrum obtained at 39°W longitude. Our inferred orthopyroxenes and clinopyroxenes contents agree with the one of Lawrence and Lucey (2007). On the other hand, we have not detected the presence of anorthite as in Lawrence and Lucey (2007). Instead, we have found a high percentage of neutral phases, such as ilminite, chromite and spinel. Our modeled spectral curve of (4) Vesta (see Fig. 5) seems to better reproduce its absorption feature located at 1.9 μm, than the one obtained by Lawrence and Lucey (2007).

Donaldson and Sprague (2009) derived the mineralogy of (4) Vesta using a spectral deconvolution algorithm. Their fit to the MIDAS[2] spectrum (see Donaldson and Sprague, 2009 for mode details, with reference to Lim et al. (2005)), obtained at 73–96°W longitude, showed that this region of (4) Vesta surface is composed by 55–65% of pyroxenes (varying from pigeonite to hypersthene and augite) and 15–25% of plagioclase and minor amounts of olivine and chromite. Our inferred modal percentage of pyroxenes are within the range presented by Donaldson and Sprague (2009), but we have inferred a higher modal abundance of neutral phases and we have also not detected the presence of plagioclase. On the other hand, their fit to the ISO[3] spectrum (see Donaldson and Sprague, 2009 for mode details, with reference to Dotto et al. (2000)), obtained at 221°W longitude, evidenced that this region of (4) Vesta surface is composed by 49–59% of pyroxenes (varying from pigeonite to augite and hypersthene), 13–23% of plagioclase, 15–25% of olivine and minor amounts of diopside and quartz. The percentage of pyroxenes found in this fit seems to be in better agreement with the percentage that we have derived, for (4) Vesta. However, we have not detected the presence of plagioclase and olivine.

The improved σ of the fits, as compared with previous studies, is a sign that space weathering and other usually unaccounted effects, as discussed here, play an important role in spectral fits.

4.4. On the quest of the genetic relationship between HED meteorites and V-type asteroids

The genetic relationship between HED meteorites and V-type asteroids has long been discussed in the literature across the years (see e.g., McCord et al., 1970; Binzel and Xu, 1993; Binzel et al., 1997, 2002; Drake, 2001; Burbine et al., 2002). Despite the recent results from the Dawn mission that strengthened this linkage (see e.g., de Sanctis et al. 2012, 2013; McSween et al. 2011, 2013),

[2] MIDAS is an acronym for Mid Infrared Asteroids Spectroscopic Survey (Lim et al., 2005).

[3] ISO is an acronym for Infrared Space Observatory (Dotto et al., 2000).

Table 10
Inferred mineralogies of V-type asteroids which have a geometric albedo value in Table 1. The uncertainties were derived following Clark et al., (2006). The values are listed in units of vol%.

Asteroid Name	Plag	Hyper	Anor	Aug	Pio	Faya	Fors	Chro	Enst	Hed	Bron	Troi	Wolla	Ilm	Phos	Spi	σ
(4) Vesta	–	35^{+1}_{0}	–	4	18^{+1}_{-1}	–	–	9^{0}_{-1}	–	2	4^{+1}_{0}	–	–	8^{+1}_{-1}	–	21^{+1}_{-1}	3.1×10^{-3}
(854) Frostia	–	–	–	8	21^{+1}_{-2}	9^{0}_{-1}	–	34^{+1}_{-2}	5^{0}_{-1}	22^{+1}_{-1}	0^{+2}_{0}	–	–	–	–	1^{+1}_{-1}	1.0×10^{-3}
(3908) Nyx	–	–	–	22^{+1}_{-1}	7	–	29^{+2}_{-2}	24^{+1}_{-1}	19^{+1}_{-1}	–	–	–	–	–	–	–	8.4×10^{-3}
(4055) Magellan	–	–	–	5	22^{+1}_{-1}	–	38^{+2}_{-2}	21^{+1}_{-1}	14	–	–	–	–	–	–	–	7.4×10^{-3}
(5604) 1992 FE	3^{+2}_{-2}	–	–	21	26^{+1}_{-1}	–	–	11	39^{+1}_{-1}	–	–	–	–	–	–	–	1.1×10^{-2}
(6611) 1993 VW	–	1	–	4	24^{+1}_{-1}	1	36^{+2}_{-2}	10	9	–	–	–	–	–	13	2	3.2×10^{-3}
(21238) Panarea	–	–	–	–	12	–	–	–	14^{+1}_{-1}	–	–	–	65	9	–	–	8.7×10^{-3}
(52750) 1998 KK17	–	18	7	–	22^{+1}_{-1}	–	29^{+2}_{-2}	15	2	8	–	–	–	–	–	–	7.7×10^{-3}
(137924) 2000 BD19	–	6^{+2}_{-2}	–	–	11^{+1}_{-1}	–	–	48^{+1}_{-1}	–	36	–	–	–	–	–	–	5.6×10^{-3}

Legend: Plag: Plagioclase; Hyper: Hypersthene; Anor: Anorthite; Aug: Augite; Pio: Pigeonite; Faya: Fayalite; Fors: Forsterite; Chro: Chromite; Enst: Enstatite; Hed: Hedenbergite; Bron: Bronzite; Troi: Troilite; Wolla: Wollastonite; Ilm: Ilmenite; Phos: Phosphates; Spi: Spinel.

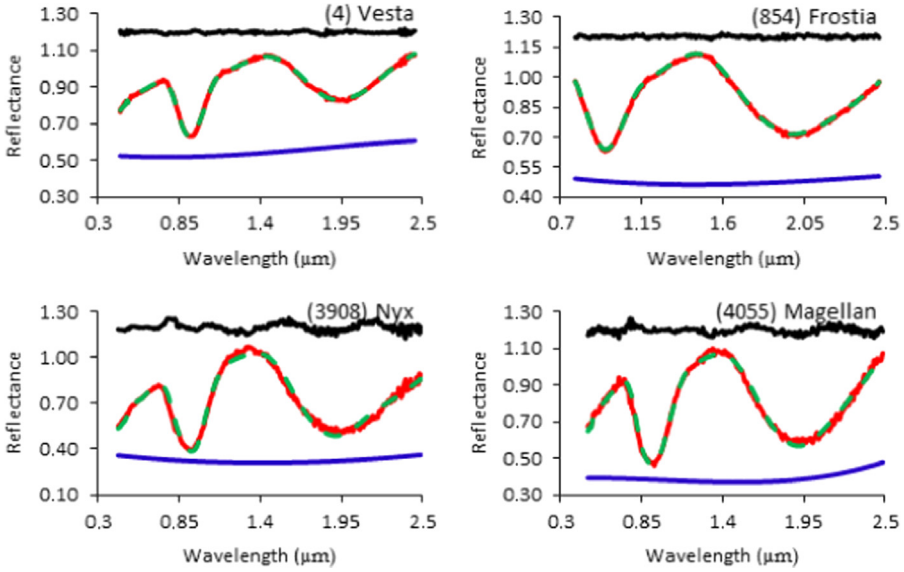

Fig. 5. Best fit model (green dashed line) of the reflectance spectra of six V-type asteroids (red line). Fit residuals (black line) were vertically shifted by: 1.2 units for (4) Vesta, (854) Frostia, (3908) Nyx and (4055) Magellan. The $U(\lambda)$ curves (blue line) were vertically shifted by: 0.85 units for (4055) Magellan; 0.9 units for (4) Vesta and (3908) Nyx; 1.1 units for (5370) Abehiroshi; and 1.2 units for (854) Frostia. The goodness of these fits are listed in Table 10. (For interpretation of the references to color in this figure legend, the reader is referred to the web version of this article.)

it is still questioned by some authors (see, e.g., Schiller et al., 2011; Wasson, 2013). We also aim to analyze this genetic linkage.

We first tried to identify possible meteoritic analogues of the selected V-type asteroids, by gathering a set of HED meteorite spectra that closely matched. We have performed a χ^2 test to find the best spectral matches for each of the asteroids listed in Table 10. We list the results of this test in Table 11. In Fig. 7, we show the best spectral match found for each asteroid. We do not show the result for (137924) 2000 BD19, as the χ^2 for the first best spectral match is too high. Based on these results, we have identified that (4) Vesta, (3908) Nyx, (4055) Magellan, (5604) 1992 FE and (6611) 1993 VW seem to have a similar mineralogy to howardites. On the other hand, we have identified that (854) Frostia and (52750) 1998 KK17 seem to have a mineralogy similar to eucrites. (21238) Panarea appears to have a mineralogy similar to a diogenite, which is in good agreement with the result pointed out by de Sanctis et al. (2011a). We have not included asteroids (286458) 2005 VW and 2003 FT3 in this analysis since we have not found their geometric albedo value in the literature.

In Fig. 8, we show a plot of clinopyroxenes versus orthopyroxenes abundances, for all the V-type asteroids listed in Table 1 which have a geometric albedo value listed. The derived mass fractions indicate that the surface of V-type asteroids and the selected HED meteorites are composed by a mixture of pyroxenes. Some traces of olivine were also found in some HED meteorites. These results strengthen the relationship between (4) Vesta, Vestoids and HED meteorites (McCord et al., 1970), as also evidenced by recent results from the DAWN mission (de Sanctis et al. 2012, 2013; McSween et al. 2011, 2013). According to our fit results for (4) Vesta and also to its position in Fig. 8, (4) Vesta's mineralogy is composed by eucritic-to-howarditic material, as also evidenced by the results from the DAWN mission (de Sanctis et al. 2013).

According to Fig. 8, (4) Vesta, (3908) Nyx, (4055) Magellan, (5604) 1992 FE and (6611) 1993 VW agree with eucritic-to-howarditic mineralogies. This evidence also confirms the linkages previously established through the χ^2 test and also shown in Fig. 7, between these five asteroids and their howardite analogues. Also, according to Burbine et al. (2009), the mineralogy of (3908) Nyx is probably similar to one of an eucrite or howardite, which is in good agreement with our results. (854) Frostia is located in the vicinity of the dynamical family of (4) Vesta. But, Zappala et al. (1995) has not included this asteroid as a member of the family of (4) Vesta. In fact, not all the objects in the vicinity of (4) Vesta belong to its family (Duffard et al., 2004). The best spectral match identified for (854) Frostia was an eucrite. Indeed, its pyroxene mineralogy is similar to the ones of eucrites (Fig. 8), but is found

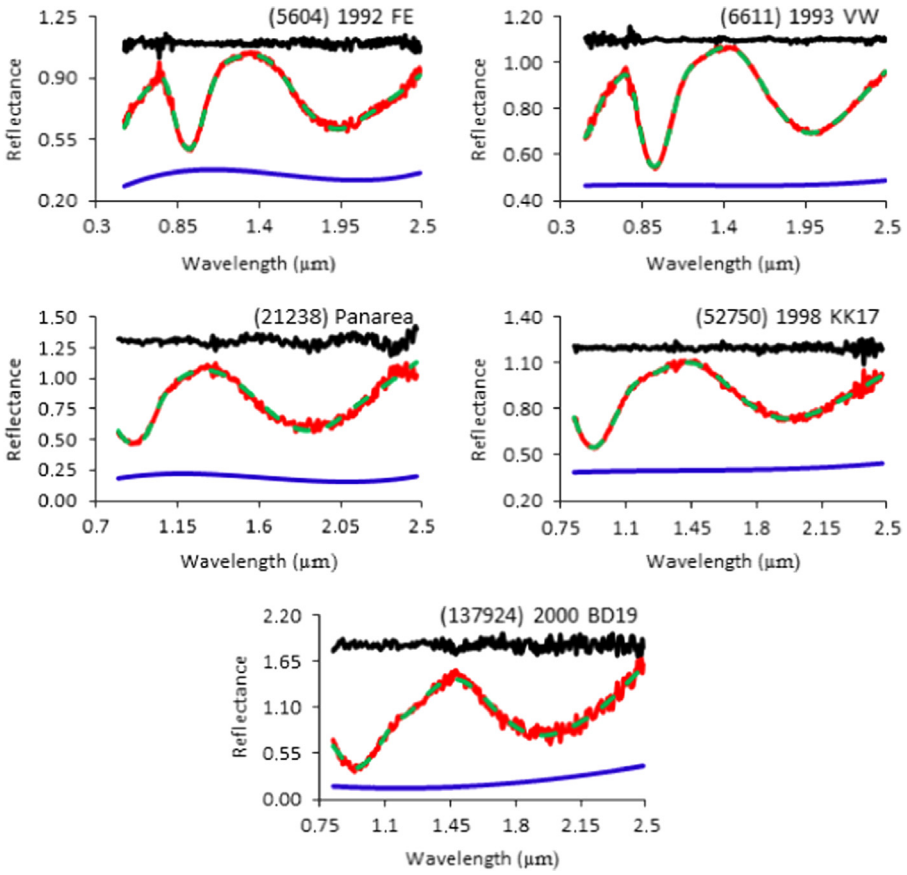

Fig. 6. Best fit model (green dashed line) of the reflectance spectra of five V-type asteroids (red line). Fit residuals (black line) were vertically shifted by: 1.1 units for (5604) 1992 FE and (6611) 1993 VW; 1.2 units for (52750) 1998 KK17; 1.3 units for (21238) Panarea; and 1.85 units (137924) 2000 BD19. The $U(\lambda)$ curves (blue line) were vertically shifted by: 0.6 units for (5604) 1992 FE; 0.9 units for (52750) 1998 KK17; 1 unit for (137924) 2000 BD19; and 0.7 units for (21238) Panarea. The goodness of these fits are listed in Table 10. (For interpretation of the references to color in this figure legend, the reader is referred to the web version of this article.)

Table 11
The three best spectral matches (BSM) for the V-type asteroids listed in Table 10. The χ^2 value of each BSM is specified in parenthesis.

Asteroid Name	BSM 1	BSM 2	BSM 3
(4) Vesta	Howardite MP-TXH-053-A (0.21)	Eucrite MP-TXH-089-A (0.88)	Eucrite MP-TXH-078-A (0.94)
(854) Frostia	Eucrite MP-TXH-119 (0.61)	Eucrite MT-HYM-030 (0.75)	Howardite MP-TXH-067-A (0.80)
(3908) Nyx	Howardite MP-TXH-126 (1.02)	Diogenite MP-TXH-071-A (1.08)	Howardite MP-TXH-082-A (1.59)
(4055) Magellan	Howardite MP-TXH-093-A (0.65)	Howardite MP-TXH-097-A (1.24)	Howardite MP-TXH-126 (1.36)
(5604) 1992 FE	Howardite MP-TXH-093-A (0.55)	Howardite MP-TXH-126 (1.00)	Howardite MP-TXH-099-A (1.09)
(6611) 1993 VW	Howardite MP-TXH-073-A (0.40)	Howardite MP-TXH-067-A (0.52)	Eucrite MP-TXH-096-A (0.54)
(21238) Panarea	Diogenite MB-TXH-095-B (0.61)	Diogenite MP-TXH-088-A (0.73)	Diogenite MP-TXH-068-A (0.73)
(52750) 1998 KK17	Eucrite MP-TXH-072-A (0.34)	Eucrite MP-TXH-119 (0.38)	Eucrite MP-TXH-121 (0.41)
(137924) 2000 BD19	Eucrite MT-HYM-033 (10.40)	Eucrite MP-TXH-054-A (10.70)	Eucrite MP-TXH-087-A (10.80)

close to the border of the 2σ region of eucrites. Despite we have not identified a meteoritic analogue for (137924) 2000 BD19 among the selected HED meteorites, this asteroid has similar pyroxene mineralogical composition similar to eucrites (Fig. 8). On the other hand, (21238) Panarea does not have a pyroxene mineralogy consistent with any HED type (Fig. 8). Actually, de Sanctis et al. (2011b) also quote that this asteroid has spectral parameters which differ from V-type asteroids in the inner belt and argue that it may be not related to (4) Vesta.

Indeed, our results not only contradict the conclusions of Schiller et al. (2011) and Wasson (2013), but also evidence that not all HED meteorites may come from (4) Vesta. There are also other V-type asteroids in the vicinity of the dynamical family of (4) Vesta that may also be plausible parent bodies of HED meteorites, as is the example of (854) Frostia. However, we do not discard the possibility that HED meteorites may also come from asteroids other than the V-type asteroids.

The collisions suffered by (4) Vesta, eventually ejected a big amount of material into its neighborhood. Some of the ejected fragments agglomerated and originated small bodies, which show a howarditic-type spectra (i.e., composed by eucritic and diogenitic material—see Fig. 8). These bodies would have formed the family of howarditic-type asteroids. In this scenario, (3908) Nyx, (4055) Magellan, (5604) 1992 FE and (6611) 1993 VW may be a result of the agglomeration of eucritic and diogenitc material after the collision suffered by (4) Vesta. On the other hand, eucritic material is quoted to have been originated from the mantle close to (4) Vesta surface (Takeda, 1997). As we linked (52750) 1998 KK17 to an eucrite, this asteroid was probably formed in the uppermost layers of (4) Vesta. Diogenitic material is postulated to

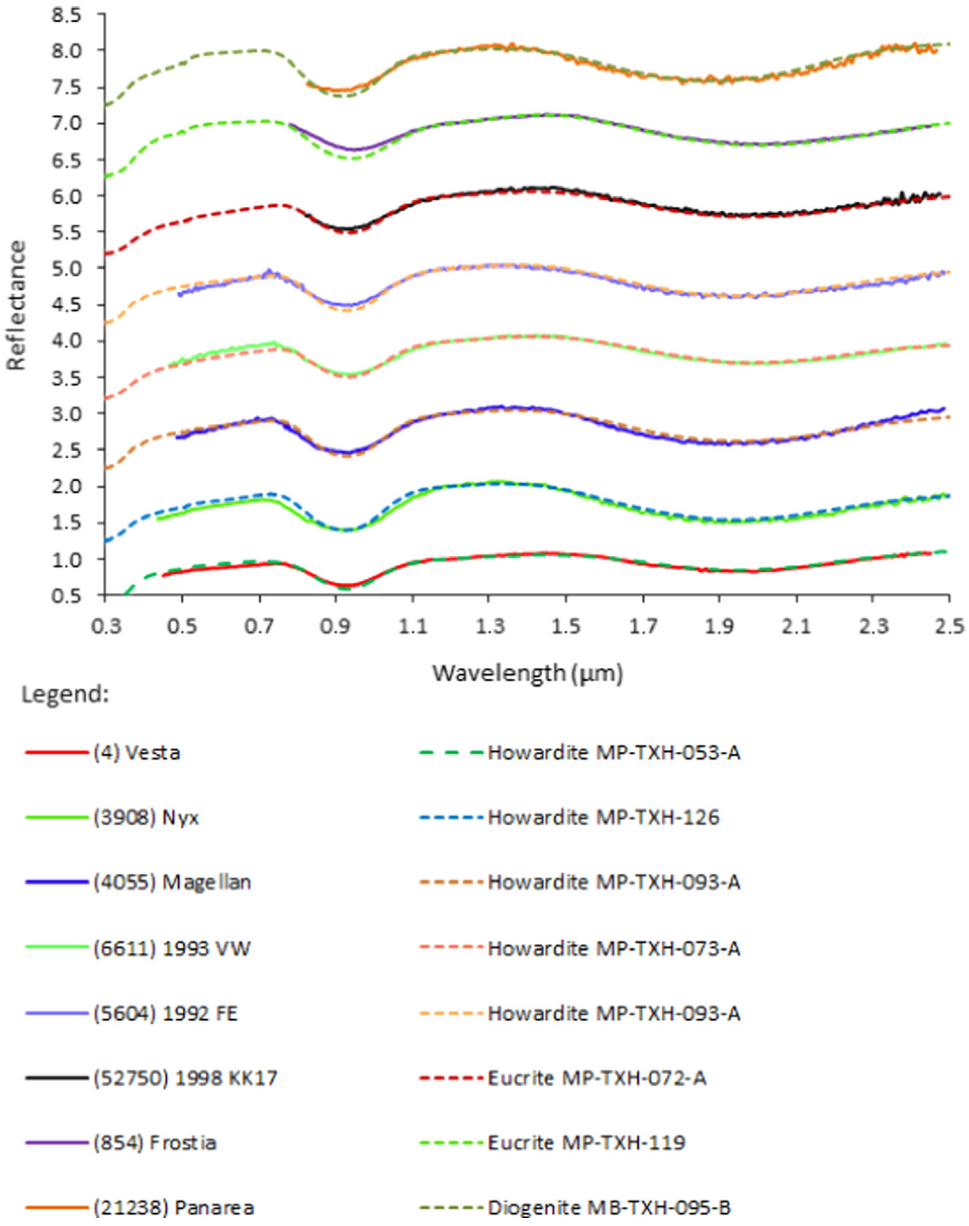

Fig. 7. Reflectance spectra of six V-type asteroids and corresponding HED with the closest mineralogy. A vertical shift of 1 unit is introduced between different groups of spectra.

be present in the innermost layers of (4) Vesta (Takeda, 1997). If the collisions suffered by (4) Vesta reached the inner layers close to the mantle, some traces of olivine might also be found in some Vestoids and HED meteorites. Actually, as evidenced by our inferred mineralogies, we have found a considerable content of olivine in almost all of the selected V-type asteroids (see Table 10) and several HED meteorites (see Table 7). Of particular interest is the amount of olivine inferred for (6611) 1993 VW, which is in agreement with the indication pointed out by Duffard et al. (2006). Such evidence may favor the magma ocean model of (4) Vesta interior (Righter and Drake, 1997).

The silicate mineralogy inferred for the studied V-type near-Earth asteroids requires that their parent body suffered early igneous differentiation in its history, producing a basaltic surface lithology (Sunshine et al., 2004). Indeed, the presence of Opx in asteroids can be considered as a tracer of their igneous history. Minerals like Opx and plagioclases were preferentially incorporated in early partial melts from a chondritic precursor and depleted in residues of partial melting (Sunshine et al., 2004). So, (4) Vesta is indeed a differentiated asteroid.

5. Conclusions

This implementation of the bidirectional Hapke radiative transfer model (Hapke, 1993) is well adapted to infer the mineralogy of V-type asteroids and HED meteorites. We have performed modal analysis on laboratorial samples, HED meteorites and V-type asteroids. The model provides globally satisfactory fits. The mineralogical compositions that we have inferred for Opx and Cpx are in good agreement with results of other authors. The advantage of using this method is that it is possible to choose a high number of reasonable end-members minerals for the modeling process and derive their respective modal abundances.

We have inferred average mineralogical compositions for eucrites (21 ± 3%of Opx, 40 ± 4% of Cpx, 10 ± 3% of olivine, 7 ± 2% of chromite, 11 ± 3% of troilite, 6 ± 1% of spinel and 3 ± 1% of plagioclase), howardites (47 ± 7% of Opx, 25 ± 4% of Cpx, 8 ± 3% of olivine, 5 ± 2% of chromite, 7 ± 3% of troilite and 6 ± 1% of spinel) and diogenites (73 ± 10% of Opx, 13 ± 2% of Cpx, 5 ± 1% of olivine, 5 ± 2% of chromite, 2 ± 2% of troilite and 2 ± 1% of spinel) suitable for comparison with future mineralogical studies of these objects.

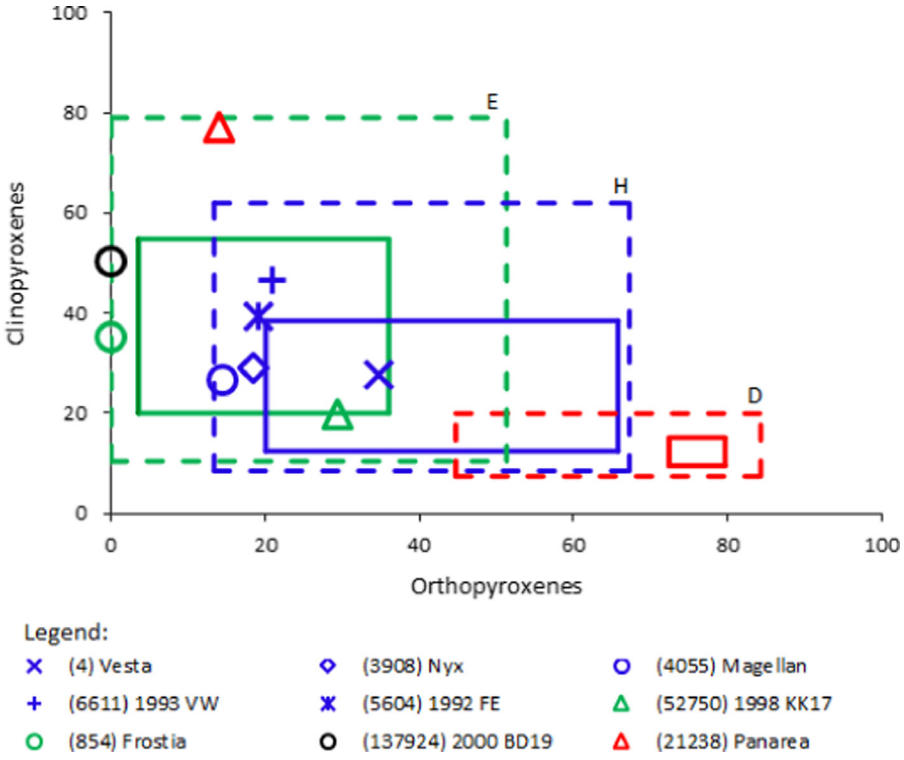

Fig. 8. Plot of the clinopyroxenes content vs orthopyroxenes content for the eleven V-type asteroids. The colored solid rectangles define the 1σ (or 1 standard deviation from the average) region of the statistical mineralogical distributions of Cpx and Opx, while the dashed colored rectangles define the 2σ (or 2 standard deviations from the average) region. The statistical mineralogical distribution of: eucrites is represented by green rectangles, howardites by blue rectangles and diogenites by red rectangles. The asteroids bullets are highlighted in red, blue or green according to their meteoritic analogue type previously indentified. For the asteroids highlighted with a black bullet, no meteoritic analogue was found. The values are listed in units of vol%. (For interpretation of the references to color in this figure legend, the reader is referred to the web version of this article.)

Our results not only contradict the evidence pointed out by Schiller et al. (2011) and Wasson (2013), but also agree with results from the Dawn mission that strengthened the linkage between (4) Vesta and HED meteorites (de Sanctis et al. 2012, 2013; McSween et al. 2011, 2013). However, we do not discard the possibility that HED meteorites may also come from other asteroids of different types. We have identified some V-type asteroids in the close vicinity of the (4) Vesta family, such as (854) Frostia, that can also be a plausible HED parent body. Our results emphasize that some of the studied near-Earth Vestoids may come from different layers of (4) Vesta, as suggested by Takeda (1997). We have confirmed that (4) Vesta, (3908) Nyx, (4055) Magellan, (5604) 1992 FE and (6611) 1993 VW have mineralogies consistent with howardites. On the other hand, we have found that (52750) 1998 KK17 and (854) Frostia have mineralogies consistent with eucrites. Also, according to our results, (21238) Panarea is also confirmed to have not a pyroxene mineralogy similar to HED meteorites and (4) Vesta.

The mineralogical analysis of the V-type asteroids evidenced that these are mainly composed by pyroxenes. We have also found a considerable content of olivine in several of the selected V-type asteroids, which can favor the magma ocean model of (4) Vesta interior (Righter and Drake, 1997).

Acknowledgements

Most of the data used in this publication were obtained and made available by the The MIT-UH-IRTF Joint Campaign for NEO Reconnaissance. The IRTF is operated by the University of Hawaii under Cooperative Agreement no. NCC 5-538 with the National Aeronautics and Space Administration, Office of Space Science, Planetary Astronomy Program. The MIT component of this work is supported by NASA grant 09-NEOO009-0001, and previously by the National Science Foundation under Grant no. 0506716. The authors would like to thank all researchers who collaborated in the RELAB and The MIT-UH-IRTF Joint Campaign for NEO Spectral Reconnaissance, who generously made their work publically available for further studies. We are also thankful to both referees, for their detailed revisions and helpful comments that much improved this paper.

References

Ammannito, E., de Sanctis, M.C., Capaccioni, F., Teresa Capria, M., Carraro, F., Combe, J.-P., Fonte, S., Frigeri, A., Joy, S.P., Longobardo, A., Magni, G., Marchi, S., McCord, T.B., McFadden, L.A., McSween, H.Y., Palomba, E., Pieters, C.M., Polanskey, C.A., Raymond, C.A., Sunshine, J.M., Tosi, F., Zambon, F., Russell, C.T., 2013. Vestan lithologies mapped by the visual and infrared spectrometer on Dawn. Meteorit. Planet. Sci. 48 (11), 2185–2198.

Binzel, R.P., Xu, S., 1993. Chips off of asteroid 4 Vesta: evidence for the parent body of basaltic achondrite meteorites. Science 260, 186–191.

Binzel, R.P., Gaffey, M.J., Thomas, P.C., Zellner, B.H., Storrs, A.D., Wells, E.N., 1997. Geologic mapping of Vesta from 1994 hubble space telescope images. Icarus 128 (1), 95–103.

Binzel, R.P., Lupishko, D., di Martino, M., Whiteley, R.J., Hahn, G.J., 2001. Physical properties of near-Earth objects. In: Bottke Jr., W.F., Cellino, A., Paolicchi, P., Binzel, R.P. (Eds.), Asteroids III. University of Arizona Press, Tucson, AZ, pp. 255–271.

Bowman, L.E., Spilde, M.N., Papike, J.J., 1997. Automated EDS modal analysis as applied to the diogenites. Meteorit. Planet. Sci. 32, 869–875.

Burbine, T.H., McCoy, T.J., Meibom, A., Gladman, B., Keil, K., 2002. Meteoritic parent bodies: their number and identification. In: Bottke Jr., W.F., Cellino, A., Paolicchi, P., Binzel, R.P. (Eds.), Asteroids III. University of Arizona Press, Tucson, AZ, pp. 653–667.

Burbine, T.H., Buchanan, P.C., Dolkar, T., Binzel, R.P., 2009. Pyroxene mineralogies of near-Earth vestoids. Meteorit. Planet. Sci. 44 (9), 1331–1341.

Burns, R.G., 1970. Crystal field spectra and evidence of cation ordering in olivine minerals. Am. Mineral. 55, 1608–1632.

Burns, R.G., 1993. Mineralogical Applications of Crystal Field Theory, second ed. Cambridge University Press, Cambridge p. 551.

Clark, B.E., Hapke, B., Pieters, C., Britt, D., 2002. Asteroid space weathering and regolith evolution. In: Bottke Jr., W.F., Cellino, A., Paolicchi, P., Binzel, R.P. (Eds.), Asteroids III, Eds. University of Arizona Press, Tucson, AZ, pp. 585–599.
Clark, B., Bus, S., Rivkin, A., McConnochie, T., Sanders, J., Shah, S., Hiroi, T., Shepard, M., 2006. E-type asteroid spectroscopy and compositional modeling. J. Geophys. Res. 109 (E2), E02201.
Cloutis, E.A., Gaffey, M.J., 1992. Pyroxene spectroscopy revisited: spectral-compositional correlations and relationship to geothermometry. J. Geophys. Res. 96, 22809–22826.
de Sanctis, M.C., Migliorini, A., Luzia Jasmin, F., Lazzaro, D., Filacchione, G., Marchi, S., Ammannito, E., Capria, M.T., 2011a. Spectral and mineralogical characterization of inner main-belt V-type asteroids. Astron. Astrophys. 533 (A77), 10.
de Sanctis, M.C., Ammannito, E., Migliorini, A., Lazzaro, D., Capria, M.T., McFadden, L., 2011b. Mineralogical characterization of some V-type asteroids, in support of the NASA Dawn mission. Mon. Not. R. Astron. Soc. 412 (4), 2318–2332.
de Sanctis, M.C., Ammannito, E., Capria, M.T., Tosi, F., Capaccioni, F., Zambon, F., Carraro, F., Fonte, S., Frigeri, A., Jaumann, R., Magni, G., Marchi, S., McCord, T.B., McFadden, L.A., McSween, H.Y., Mittlefehldt, D.W., Nathues, A., Palomba, E., Pieters, C.M., Raymond, C.A., Russell, C.T., Toplis, M.J., Turrini, D., 2012. Spectroscopic characterization of mineralogy and its diversity across Vesta. Science 336 (6082) (697-690).
de Sanctis, M.C., Ammannito, E., Capria, M.T., Capaccioni, F., Combe, J.-P., Frigeri, A., Longobardo, A., Magni, G., Marchi, S., McCord, T.B., Palomba, E., Tosi, F., Zambon, F., Carraro, F., Fonte, S., Li, Y.J., McFadden, L.A., Mittlefehldt, D.W., Pieters, C.M., Jaumann, R., Stephan, K., Raymond, C.A., Russell, C.T., 2013. Vesta's mineralogical composition as revealed by the visible and infrared spectrometer on Dawn. Meteorit. Planet. Sci. 48 (11), 2166–2184.
Dotto, E., Müller, T.G., Barucci, M.A., Encrenaz, T., Knacke, R.F., Lellouch, E., Doressoundiram, A., Crovisier, J., Brucato, J.R., Colangeli, L., Mennella, V., 2000. ISO results on bright Main Belt asteroids: PHT-S observations. Astron. Astrophys. 358, 1133–1141.
Donaldson Hanna, K., Sprague, A.L., 2009. Vesta and the HED meteorites: mid-infrared modeling of minerals and their abundances. Meteorit. Planet. Sci. 44 (11), 1755–1770.
Drake, M.J., 2001. The eucrite—Vesta story. Meteorit. Planet. Sci. 36 (4), 501–513.
Duffard, R., Lazzaro, D., Licandro, J., de Sanctis, M.C., Capria, M.T., Carvano, J.M., 2004. Mineralogical characterization of some basaltic asteroids in the neighborhood of (4) Vesta: first results. Icarus, 171; , pp. 120–132.
Duffard, R., de Léon, J., Licandro, J., Lazzaro, D., Serra-Ricart, M., 2006. Basaltic asteroids in the near-Earth objects population: a mineralogical analysis. Astron. Astrophys. 456, 775–781.
Hapke, B., 1993. Theory of Reflectance and Emittance Spectroscopy, first ed. Cambridge University Press, New York.
Hiroi, T., Binzel, R.P., Sunshine, J.M., Pieters, C.M., Takeda, H., 1995. Grain sizes and mineral compositions of surface regoliths of Vesta-like asteroids. Icarus 115, 374–386.
Klima, R.L., Pieters, C.M., Dyar, M.D., 2007. Spectroscopy of synthetic Mg-Fe pyroxenes I: spin-allowed and spin-forbidden crystal field bands in the visible and near-infrared. Meteorit. Planet. Sci. 42, 235–253.
Lawrence, S.J., Lucey, G., 2007. Radiative transfer mixing models of meteoritic assemblages. J. Geophys. Res. 112, E07005.
Lim, L.F., McConnochie, T.H., Bell III, J.F., Hayward, T.L., 2005. Thermal infrared (8–13 μm) spectra of 29 asteroids: the Cornell mid-infrared asteroid spectroscopy (MIDAS) survey. Icarus 173, 385–408.
Lucey, P., 1998. Model near-infrared optical constants of olivines and pyroxene as a function of iron content. J. Geophys. Res. 103, 1703–1713.
McCord, T.B., Adams, J.B., Johnson, T.V., 1970. Asteroid Vesta: spectral reflectivity and compositional implications. Science 168 (3938), 1445–1447.
McSween, H.Y., Mittlefehldt, D.W., Beck, A.W., Mayne, R.G., McCoy, T.J., 2011. HED meteorites and their relationship to the geology of Vesta and the dawn mission. Space Sci. Rev. 163 (1-4), 141–174.
McSween, H.Y., Binzel, R.P., de Sanctis, M.C., Ammannito, E., Prettyman, T.H., Beck, A.W., Reddy, V., Corre, L., Gaffey, M.J., McCord, T.B., Raymond, C.A., Russell, C.T., 2013. Dawn; the Vesta-HED connection; and the geologic context for eucrites, diogenites, and howardites. Meteorit. Planet. Sci. 48 (11), 2090–2104.
Morimoto, N., Fabries, J., Ferguson, A.K., Ginzburg, I.V., Ross, M., Seifeit, F.A., Zussman, J., 1989. Nomenclature of pyroxenes. Can. Mineral. 27, 143–156.
Mustard, J.F., Pieters, C.M., 1989. Photometric phase functions of common geologic materials and applications to quantitative analysis of mineral mixture reflectance spectra. J. Geophys. Res. 94 (13), 619–634.
Nelson, M.L., Britt, D.T., Lebofsky, L., 1993. Mineralogy of asteroids compositions. Resour. Near-Earth Space, 493–522.
Papike, J.J., Shearer, C.K., Spilde, M.N., Karner, J.M., 2000. Metamorphic diogenite Grosvenor Mountains 95555: mineral chemistry of orthopyroxene and spinel and comparisons to the diogenite suite. Meteorit. Planet. Sci. 35 (4), 875–879.
Pieters, C.M., Hiroi, T., 2004. RELAB (Reflectance Experiment Laboratory): A NASA Multi-user Spectroscopy Facility. LPS, 35, Abstract #1720 (CDROM).
Rayner, J.T., Tooney, D.W., Onaka, P.M., Denault, A.J., Stahlberger, W.E., Vacca, W.D., Cushing, M.C., Wang, S., 2003. SpeX: a medium-resolution 0.8–5.5 μm spectrograph and imager for the NASA infrared telescope facility. Publ. Astron. Soc. Pac. 115 (805), 362–382.
Righter, K., Drake, M.J., 1997. A magma ocean on Vesta: core formation and petrogenesis of eucrites and diogenites. Meteorit. Planet. Sci. 32, 929–944.
Russell, C.T., Raymond, C.A., Coradini, A., McSween, H.Y., Zuber, M.T., Nathues, A., De Sanctis, M.C., Jaumann, R., Konopliv, A.S., Preusker, F., Asmar, S.W., Park, R.S., Gaskell, R., Keller, H.U., Mottola, S., Roatsch, T., Scully, J.E.C., Smith, D.E., Tricarico, P., Toplis, M.J., Christensen, U.R., Feldman, W.C., Lawrence, D.J., McCoy, T.J., Prettyman, T.H., Reedy, R.C., Sykes, M.E., Titus, T.N., 2012. Dawn at Vesta: testing the protoplanetary paradigm. Science 336, 684–686.
Schiller, M.J., Baker, J., Creech, J., Paton, C., Millet, M.-A., Bizzaro, M., 2011. Rapid timescales for magma ocean crystallization on the howardite-eucrite-diogenite parent body. Astrophys. J. 740, L22.
Sunshine, J., Pieters, C., Pratt, S., 1990. Deconvolution of mineral absoprtion bands: an improved approach. J. Geophys. Res. 95, 6955–6966.
Sunshine, J.M., Bus, S.J., McCoy, T.J., Burbine, T.H., Corrigan, C.M., Binzel, R.P., 2004. Hgh-calcium pyroxene as an indicator of igneous differentiation in asteroids and meteorites. Meteorit. Planet. Sci. 39 (8), 1343–1357.
Takeda, H., 1997. Mineralogical records of early planetary process on the HED parent body with reference to Vesta. Meteorit. Planet. Sci. 32, 834–853.
Wasson, J.T., Wetherill, G.W., 1979. Dynamical Chemical and Isotopic Evidence Regarding the Formation Locations of Asteroids and Meteorites. In: Asteroids. (A80-24551 08-91) Tucson, AZ, University of Arizona Press, 926-974.
Wasson, J.T., 2013. Vesta and extensively melted asteroids: why HED meteorites are probably not from Vesta. Earth Planet. Sci. Lett. 381, 138–146.
Zappala, V., Bendjoya, P., Cellino, A., Farinella, P., Froeschle, C., 1995. Asteroid families: search of a 12487 asteroid sample using two different clustering techniques. Icarus 116, 291–314.
Zema, M., Domeneghetti, M.C., Molin, G.M., Tazzoli, V., 1997. Cooling rates of diogenites: a study of Fe2+-Mg ordering in orthopyroxene by X-ray single-crystal diffraction. Meteorit. Planet. Sci. 32, 855–862.